ARMY RESEARCH LABORATORY

Chemical Reaction Equilibrium in Nanoporous Materials: NO Dimerization Reaction in Carbon Slit Nanopores

by Martin Lísal, John K. Brennan, and William R. Smith

ARL-RP-147 **September 2006**

A reprint from the *Journal of Chemical Physics*, vol. 124, pp. 064712-1–064712-14, 2006.

NOTICES

Disclaimers

The findings in this report are not to be construed as an official Department of the Army position unless so designated by other authorized documents.

Citation of manufacturer's or trade names does not constitute an official endorsement or approval of the use thereof.

Destroy this report when it is no longer needed. Do not return it to the originator.

Army Research Laboratory
Aberdeen Proving Ground, MD 21005-5066

ARL-RP-147 **September 2006**

Chemical Reaction Equilibrium in Nanoporous Materials: NO Dimerization Reaction in Carbon Slit Nanopores

Martin Lísal
Institute of Chemical Process Fundamentals, Czech Republic

John K. Brennan
Weapons and Materials Research Directorate, ARL

William R. Smith
University of Ontario Institute of Technology, Canada

A reprint from the Journal of Chemical Physics, vol. 124, pp. 064712-1–064712-14, 2006.

REPORT DOCUMENTATION PAGE

Form Approved
OMB No. 0704-0188

1. REPORT DATE *(DD-MM-YYYY)*	2. REPORT TYPE	3. DATES COVERED (From - To)
September 2006	Reprint	October 2005–February 2006

4. TITLE AND SUBTITLE
Chemical Reaction Equilibrium in Nanoporous Materials: NO Dimerization Reaction in Carbon Slit Nanopores

5a. CONTRACT NUMBER

5b. GRANT NUMBER

5c. PROGRAM ELEMENT NUMBER

6. AUTHOR(S)
Martin Lísal,[*] John K. Brennan, and William Smith[†]

5d. PROJECT NUMBER
H4311

5e. TASK NUMBER

5f. WORK UNIT NUMBER

7. PERFORMING ORGANIZATION NAME(S) AND ADDRESS(ES)
U.S. Army Research Laboratory
ATTN: AMSRD-ARL-WM-BD
Aberdeen Proving Ground, MD 21005-5066

8. PERFORMING ORGANIZATION REPORT NUMBER
ARL-RP-147

9. SPONSORING/MONITORING AGENCY NAME(S) AND ADDRESS(ES)

10. SPONSOR/MONITOR'S ACRONYM(S)

11. SPONSOR/MONITOR'S REPORT NUMBER(S)

12. DISTRIBUTION/AVAILABILITY STATEMENT
Approved for public release; distribution is unlimited.

13. SUPPLEMENTARY NOTES
[*]E. Hála Laboratory of Thermodynamics, Institute of Chemical Process Fundamentals, Academy of Sciences of the Czech Republic, 165 02 Prague 6-Suchdol, Czech Republic and Department of Physics, Institute of Science, J. E. Purkinje University, 400 96 Ústí nad Labem, Czech Republic
[†]Faculty of Science, University of Ontario Institute of Technology, 2000 Simcoe St., North Oshawa, Ontario L1H7K4, Canada
A reprint from the *Journal of Chemical Physics*, vol. 124, pp. 064712–064712-1–14, 2006

14. ABSTRACT
We present a molecular-level simulation study of the effects of confinement on chemical reaction equilibrium in nanoporous materials. We use the reaction ensemble Monte Carlo (RxMC) method to investigate the effects of temperature, nanopore size, bulk pressure, and capillary condensation on the nitric oxide dimerization reaction in a model carbon slit nanopore in equilibrium with a bulk reservoir. In addition to the RxMC simulations, we also utilize the molecular-dynamics method to determine self-diffusion coefficients for confined nonreative mixtures of nitric oxide monomers and dimmers at compositions obtained from the RxMC simulations. We analyze the effects of the temperature, nanopore width, bulk pressure, and capillary condensation on the reaction equilibrium with respect to the reaction conversion, fluid structure, and self-diffusion coefficients. We show that the influence of the temperature, nanopore size, and capillary condensation on the confined reaction equilibrium is quite dramatic while the effect of the bulk pressure on the reaction equilibrium in the carbon slit nanopore is only moderate. The work is an extension of previous work by Turner et al. [J. Chem. Phys. **114**, 1851 (2001)] on the confined reactive nitric oxide system.

15. SUBJECT TERMS
molecular simulation, Monte Carlo, reaction ensemble

16. SECURITY CLASSIFICATION OF:			17. LIMITATION OF ABSTRACT	18. NUMBER OF PAGES	19a. NAME OF RESPONSIBLE PERSON
a. REPORT	b. ABSTRACT	c. THIS PAGE			J. K. Brennan
UNCLASSIFIED	UNCLASSIFIED	UNCLASSIFIED	UL	20	19b. TELEPHONE NUMBER (*Include area code*) 410-306-0678

Chemical reaction equilibrium in nanoporous materials: NO dimerization reaction in carbon slit nanopores

Martin Lísal[a)]
E. Hála Laboratory of Thermodynamics, Institute of Chemical Process Fundamentals, Academy of Sciences of the Czech Republic, 165 02 Prague 6-Suchdol, Czech Republic and Department of Physics, Institute of Science, J. E. Purkinje University, 400 96 Ústí nad Labem, Czech Republic

John K. Brennan
U.S. Army Research Laboratory, Weapons and Materials Research Directorate, Aberdeen Proving Ground, Maryland 21005-5066

William R. Smith
Faculty of Science, University of Ontario Institute of Technology, 2000 Simcoe Street, North Oshawa, Ontario L1H7K4, Canada

(Received 3 November 2005; accepted 6 January 2006; published online 14 February 2006)

We present a molecular-level simulation study of the effects of confinement on chemical reaction equilibrium in nanoporous materials. We use the reaction ensemble Monte Carlo (RxMC) method to investigate the effects of temperature, nanopore size, bulk pressure, and capillary condensation on the nitric oxide dimerization reaction in a model carbon slit nanopore in equilibrium with a bulk reservoir. In addition to the RxMC simulations, we also utilize the molecular-dynamics method to determine self-diffusion coefficients for confined nonreactive mixtures of nitric oxide monomers and dimers at compositions obtained from the RxMC simulations. We analyze the effects of the temperature, nanopore width, bulk pressure, and capillary condensation on the reaction equilibrium with respect to the reaction conversion, fluid structure, and self-diffusion coefficients. We show that the influence of the temperature, nanopore size, and capillary condensation on the confined reaction equilibrium is quite dramatic while the effect of the bulk pressure on the reaction equilibrium in the carbon slit nanopore is only moderate. This work is an extension of previous work by Turner *et al.* [J. Chem. Phys. **114**, 1851 (2001)] on the confined reactive nitric oxide system.
 [DOI: 10.1063/1.2171213]

I. INTRODUCTION

With the rapid growth of nanotechnology and the invention of various nanoporous materials, some of these materials have been proposed as vehicles for nanochemical devices such as nanoscale reactors and nanoscale membrane reactors.[1] However, further development of these applications is impossible without a fundamental understanding of the thermodynamic, reaction, adsorption, and transport mechanisms of fluids confined in nanopores.

We now have a fairly good understanding of the influence of confinement on the physical properties of nanophases for simple and moderately complex nonreactive fluids.[2,3] It is well established, for example, that confinement brings about drastic changes in the thermodynamic properties of nonreactive fluids such as narrowing the vapor-liquid coexistence curve, lowering the pore critical temperature, increasing the average fluid densities in pores, and the appearance of new types of phase transitions not found in the bulk phase.

By contrast, significantly less is known about the effects of confinement on chemical properties, particularly on chemical reaction equilibria. A chemical reaction, confined to a nanosized environment, can have a different outcome as compared to the same reaction in the bulk phase. For example, generally the nanopore phase has a higher density than the corresponding bulk phase; based upon Le Chatelier's principle this results in an increase in yield for reactions in which there is a decrease in the total number of moles. Conversely, a drop in yield occurs in reactions where the number of moles increases. Further, some components of the reactive mixture are selectively adsorbed on the solid surfaces, subsequently affecting the reaction equilibrium. Still further, molecular orientations can be strongly influenced by proximity to a solid surface which can also shift the reaction equilibrium relative to the bulk phase equilibrium. Finally, phase transitions such as capillary condensation are expected to have a strong influence on the reaction conversion in the nanopores.

Molecular-level simulation studies of the effects of confinement on reaction equilibria were pioneered by Borówko *et al.*[4] and Borówko and Zagórski[5] for model, reversible reactions in slit pores and by Turner *et al.*[6–8] for realistic, reversible reactions (nitric oxide dimerization and ammonia synthesis) in carbon micropores and carbon nanotubes. The

[a)]Author to whom correspondence should be addressed; mailing address: E. Hála Laboratory of Thermodynamics, Institute of Chemical Process Fundamentals, Academy of Sciences of the Czech Republic, Rozvojová 135, 165 02 Prague 6-Suchdol, Czech Republic. Electronic mail: lisal@icpf.cas.cz

study by Turner *et al.*[6] was inspired by the experimental work of Kaneko *et al.*[9] and Nishi *et al.*[10] who attempted to experimentally measure reaction equilibria in carbon nanopores. More recently, Peng *et al.*[11] simulated chemical reaction equilibria of ammonia synthesis in two porous materials (MCM-41 and pillared clays) and Hansen *et al.*[12] simulated the reaction equilibria of a metathesis reaction system in silicalite-1 pores.

All the above-mentioned simulations mainly focused on the influence of the pore size on the reaction conversion. In addition, they also considered the effects of chemical and physical surface heterogeneities on the reaction conversion, as well as the influence of the variation of the equilibrium constant across the pore on the reaction equilibrium. These authors employed the reaction ensemble Monte Carlo (RxMC) simulation technique[13–15] that enables one to directly simulate the equilibrium properties of chemically reacting systems. The method requires only a knowledge of the reaction species intermolecular potentials and their ideal-gas properties, in addition to specifying the system stoichiometry and the thermodynamic constraints.

While dramatically influencing the thermodynamic properties, confinement also affects the transport properties of fluids inside nanopores. Moreover, confinement contributes significantly to both the thermodynamic and transport properties if chemical reactions and mixture separation are occurring simultaneously in the nanoporous materials. Physical space restrictions based on the fluid particle size or structure may limit the flow of particles through particular nanopores in the material. Furthermore, attraction of the nanopore surface, i.e., physisorption, may play a critical role. Even further complicating matters, fluid particles may chemisorb. In addition to phenomena occurring between fluid particles and the nanopore surface, the transport behavior in the nanoporous material becomes increasingly more complex if chemical reactions occur between fluid particles.

Recently, we proposed a novel simulation tool for such scenarios, termed the dual control cell reaction ensemble molecular-dynamics (DCC-RxMD) method.[16,17] The DCC-RxMD method simulates fluid mixtures that are simultaneously chemically reacting and adsorbing in a nanoporous material by coupling a nonequilibrium molecular-dynamics method with the RxMC and grand canonical ensemble Monte Carlo methods. The simulation setup mimics an experimental system where the control cells that maintain the desired reaction and flow conditions are in direct physical contact with the adsorbing media. The DCC-RxMD method was applied to the dry reforming of methane reaction in model nanoscale membrane reactors.[16] These DCC-RxMD simulation studies provided unique insight into the effects of the membrane structure and porosity and imposed pressure gradients on the reaction conversion.

In addition to these simulation and experimental studies, density-functional theory (DFT) studies on model dimerization reactions in slit pores have also been performed.[18] Tripathi and Chapman extended the DFT method developed by Chapman and co-workers for confined associating systems[19,20] to the study of confined dimerization reactions. They studied the effects of the pore size and capillary condensation on the reaction equilibrium. DFT predicts an increase in the reaction conversion due to capillary condensation, with the impact being most significant in the smaller pores.

In this paper, we continue the work of Turner *et al.*[6] on the nitric oxide dimerization reaction, $2NO \rightleftharpoons (NO)_2$, in model carbon slit nanopores. However, motivated by the findings of the DFT studies by Tripathi and Chapman,[18] we shift our focus to the effects of bulk pressure and capillary condensation on the confined reaction equilibrium and fluid structure. To provide further insight, we report self-diffusion coefficients obtained from MD simulations of confined nonreactive mixtures of nitric oxide monomers and dimers at compositions determined from RxMC simulations. More in-depth studies of the transport properties of this system will be considered in subsequent work. For these future studies the implementation of the aforementioned DCC-RxMD method will be necessary.

Besides being studied previously, the nitric oxide dimerization reaction is interesting for a number of reasons. The reaction is an exothermic, thermodynamically driven reaction in which there is a decrease in the total number of moles. The reaction is important in atmospheric chemistry as well as in the human body where it regulates blood pressure. Moreover, predicting the effects of confinement on NO dimerization is critical to pollution abatement since activated carbons are commonly used for the removal of nitrogen oxides from autoexhaust and industrial effluent gas streams. From a modeling standpoint, the NO dimerization reaction in carbon slit nanopores is an ideal reaction to simulate. Carbon nanopores exhibit quite strong solid-fluid interactions[2,3] and the molecules involved in the reaction, NO and $(NO)_2$, are simple and easy to model. Due to the NO paramagnetism and $(NO)_2$ diamagnetism, the composition of the reactive mixture in activated carbons can be measured by magnetic susceptibility,[9] providing experimental data for comparison.

The paper is organized as follows. The simulation methodology is described in Sec. II along with the simulation details. Molecular models for fluid-fluid and solid-fluid interactions together with the evaluation of the equilibrium constant are presented in Sec. III. Results are discussed in Sec. IV. Finally, Sec. V gives our conclusions.

II. SIMULATION METHODOLOGY

In this work, we used the RxMC method to simulate the reaction equilibrium of the $2NO \rightleftharpoons (NO)_2$ system in a model carbon slit nanopore in equilibrium with a bulk reservoir. Constant-temperature–constant-volume (*NVT*) MD simulations were carried out to determine the self-diffusion coefficients of the corresponding confined $NO/(NO)_2$ equilibrium mixture. We assessed the dependency of the reaction equilibria and self-diffusion coefficients on various factors, including the nanopore width, bulk reservoir pressure, temperature, and capillary condensation. For each case, the fluid structure was analyzed by constructing density profiles of each species in the nanopore.

A. Reaction ensemble Monte Carlo

The RxMC method[13–15] is a powerful simulation tool for studying chemically reacting mixtures. The method only requires inputting the intermolecular potentials and the ideal-gas properties of the reaction species that are present. Most notably, the method does not require a reactive-type potential that mimics bond breakage and formation, see e.g., Refs. 21 and 22. Reactions are simulated by performing forward and reverse reaction steps according to the RxMC algorithm which guarantees that the reaction equilibrium criteria for a set of R linearly, independent chemical reactions

$$\sum_{i=1}^{c} \nu_{ji}\mu_i = 0, \quad j = 1,2, \ldots, R \tag{1}$$

are established.[23] In Eq. (1), ν_{ji} is the stoichiometric coefficient of species i in chemical reaction j and μ_i is its chemical potential. The reaction equilibrium condition for our NO dimerization reaction $2\mathrm{NO} \rightleftharpoons (\mathrm{NO})_2$ is then

$$\mu_{(\mathrm{NO})_2} - 2\mu_{\mathrm{NO}} = 0. \tag{2}$$

Forward and reverse reaction steps are accepted with probabilities

$$\min\left[1, \frac{\Gamma}{V}\frac{N_{\mathrm{NO}}(N_{\mathrm{NO}}-1)}{N_{(\mathrm{NO})_2}+1}\exp\left(-\frac{\Delta U}{k_{\mathrm{B}}T}\right)\right] \tag{3}$$

and

$$\min\left[1, \frac{V}{\Gamma}\frac{N_{(\mathrm{NO})_2}}{(N_{\mathrm{NO}}+1)(N_{\mathrm{NO}}+2)}\exp\left(-\frac{\Delta U}{k_{\mathrm{B}}T}\right)\right], \tag{4}$$

respectively. In Eqs. (3) and (4), V is the system volume, T is the temperature, N_i is the number of particles of species i, k_{B} is Boltzmann's constant, Γ is the ideal-gas quantity defined as

$$\Gamma = \frac{k_{\mathrm{B}}T}{P^0}K, \tag{5}$$

P^0 is the standard-state pressure (taken to be 1 bar), ΔU is the change in the configurational energy U due to forward and reverse reaction attempts, and K is the equilibrium constant.

Reaction steps and standard Monte Carlo displacement moves[24,25] were carried out in both the bulk and nanopore phases. The simulation of a nanopore phase in equilibrium with a bulk reservoir phase requires volume changes for the bulk phase along with particle interchanges between the nanopore and bulk phases.[26] Particle exchanges between the phases were only performed for the NO monomer, which is the smaller of the molecules in the dimerization reaction.[6]

The nanopore consisted of two structureless confining walls separated by a distance H in the z direction with periodic boundary conditions applied in the x and y directions only. The bulk phase was represented by a cubic simulation box where the minimum image convention and periodic boundary conditions were applied. In the case of the nanopore phase, a cutoff equal to half the maximum box size was utilized where the long-range correction for the configurational energy was ignored. In the case of the bulk phase, a spherical cutoff radius equal to half the box length was used and the long-range correction for the configurational energy was included,[24] assuming that the radial distribution function is unity beyond the cut-off radius.

The simulations were initiated by randomly placing NO molecules into the nanopore and bulk simulation boxes. The initial number of NO molecules was chosen such that a statistically reasonable number of molecules ($\sim$500) were present in the bulk phase once the system had equilibrated. The RxMC simulations were organized in cycles as follows. Each cycle consisted of four steps: n_D displacement moves (translation or rotation), n_V volume moves for the bulk phase, n_ξ reaction moves, and n_T NO molecule transfers. The four types of moves were selected at random with fixed probabilities, chosen such that the ratio $n_D{:}n_V{:}n_\xi{:}n_T$ in each cycle was $\bar{N}{:}1{:}\bar{N}{:}\bar{N}$, where $\bar{N}$ was about 10%–20% greater than the equilibrium number of molecules during a simulation run. The acceptance ratios for translational and rotational moves, and for volume changes, were adjusted to be approximately 30%. After an equilibration period, we typically generated 6×10^4 cycles to accumulate averages of the desired quantities. The precision of the simulated data was obtained using block averages, with 5000 cycles/block. In addition to ensemble averages of the quantities of direct interest, we also carefully monitored the convergence profiles of the thermodynamic quantities as the system traveled through phase space.[27]

B. Molecular dynamics

After determining the reaction equilibrium concentrations in the nanopore phase from RxMC simulations, the transport properties of these fluid mixtures were determined using the following approach. A fluid mixture matching the final average concentrations from the RxMC simulation was created in the nanopore. We then employed a standard *NVT* MD method[24,25] to simulate particle movements trough time space. Since a smooth potential was used to represent the graphite planes (as opposed to an atomistically detailed representation), we needed to account for the exchange of momentum which would take place between fluid molecules and the carbon atoms. Therefore, within the MD method framework we implemented the so-called diffuse boundary condition based on the work of Travis and Gubbins[28] as follows. After each MD time step we monitored whether the following two conditions were satisfied: (i) the center-of-mass momentum of a given molecule in the direction perpendicular to the wall has reversed in sign and (ii) the center-of-mass momentum of that same molecule was within the repulsive region of the solid-fluid potential. If, and only if, both of these conditions were satisfied, then we reselect the center-of-mass momentum of that molecule in the directions parallel to the confining walls from a Maxwell-Boltzmann distribution corresponding to the prescribed temperature.[24] Such an approach does not alter the angular velocity of molecules that are approximately spherical-like and diffusing at moderate to high temperatures (both approximations are satisfied in this study).

The equations of motion in the *NVT* MD method were

solved using the leap-frog algorithm[24] and by implementing the damped force method of Brown and Clark[29] and Fincham[30] along with the Berendsen thermostat[31] to maintain constant temperature. A time step of $\Delta t=2.5$ fs and a coupling time constant $\tau_T=0.01$ ps in the Berendsen thermostat were used for a total simulation time of 1 ns following an equilibration period.

During the course of the *NVT* MD simulation, we evaluated mean-square displacements in directions parallel to the walls, denoted as MSD^i_α, where $\alpha \equiv (x,y)$ and $i \equiv [\mathrm{NO},(\mathrm{NO})_2]$. MSD^i_α values were used to calculate self-diffusion coefficients in one dimension, D^i_α, by means of the Einstein equation,[24] where

$$D^i_\alpha = \lim_{t\to\infty} \frac{\mathrm{MSD}^i_\alpha}{2t} \tag{6}$$

and

$$\mathrm{MSD}^i_\alpha = \langle \Delta\alpha^i(t) \rangle = \left\langle \frac{1}{N_i} \sum_{j=1}^{N_i} |\alpha^i_j(t) - \alpha^i_j(0)|^2 \right\rangle. \tag{7}$$

In Eqs. (6) and (7), t is the time, α^i_j is a component of the unfolded position of a molecule j (i.e., not subject to periodic boundary conditions), and $\langle\cdot\rangle$ is the appropriate ensemble average. In a slit nanopore, D^i_x and D^i_y should be the same within simulation uncertainties and we thus report one-dimensional self-diffusion coefficients, D^i, as average values of the corresponding D^i_x and D^i_y quantities.

III. MOLECULAR MODEL

A. Fluid-fluid interaction

As in the previous simulation studies of the NO dimerization reaction,[6,14] we used the model proposed by Kohler *et al.*[32] to describe intermolecular interactions in the mixture of NO and $(\mathrm{NO})_2$. The model treats NO as a single Lennard-Jones (LJ) sphere and $(\mathrm{NO})_2$ as a two-site LJ molecule with the bond length l equal to the experimental value of 0.2237 nm. For the monomer, the model uses the LJ energy parameter $\varepsilon/k_\mathrm{B}=125.0$ K and the LJ size parameter $\sigma=0.317\,15$ nm. The individual LJ parameters for each site in the dimer are the same as those for the monomer. Due to the weak dipole and quadrupole moments, the model neglects electrostatic forces.

B. Solid-fluid interaction

When simulating equilibrium fluid properties in carbon slit nanopores, it is possible to treat the walls as structureless.[2] In this case, a solid-fluid intermolecular potential is obtained by replacing the sum over solid-fluid particle interactions by a sum of integrals over wall atoms in a given plane. This is a reasonable approximation when the fluid molecule is large compared with the spacing between wall atoms. In graphitic carbons, the C–C spacing between surface carbon atoms is about 0.142 nm and molecules such as NO ($\sigma=0.317\,15$ nm) or $(\mathrm{NO})_2$ ($\sigma=0.317\,15$ nm, $l=0.2237$ nm) feel only a rather small corrugation in the solid-fluid interaction as it moves parallel to the surface. Assuming a LJ potential for the wall atom-fluid interaction and integrating over the interactions with individual carbon atoms in each graphite plane, Steele[33] obtained the 10-4-3 potential for the interaction of a fluid atom with the graphite wall,

$$u_\mathrm{sf}(z) = 2\pi\varepsilon_\mathrm{sf}\sigma^2_\mathrm{sf}\rho_s\Delta\left[\frac{2}{5}\left(\frac{\sigma_\mathrm{sf}}{z}\right)^{10} - \left(\frac{\sigma_\mathrm{sf}}{z}\right)^4 - \frac{\sigma^4_\mathrm{sf}}{3\Delta(z+0.61\Delta)^3}\right]. \tag{8}$$

In Eq. (8), z is the distance of the fluid atom from the graphite surface, ε_sf and σ_sf are the LJ potential parameters for the solid-fluid interaction, $\Delta=0.335$ nm is the interplanar spacing in graphite, and $\rho_s=114$ nm^{-3} is the number density of carbon atoms. The ε_sf and σ_sf parameters are obtained from the Lorentz-Berthelot mixing rules[24] with the carbon LJ potential parameters $\varepsilon_\mathrm{ss}/k_\mathrm{B}=28$ K and $\sigma_\mathrm{ss}=0.340$ nm.

For a slit nanopore of width H, the fluid molecule interacts with both graphite walls so that the total solid-fluid interaction is given as the sum of $u_\mathrm{sf}(z)$ and $u_\mathrm{sf}(H-z)$. As an example, the solid-fluid interaction potential for the NO monomer in the model carbon slit nanopore of various widths is shown in Fig. 1.

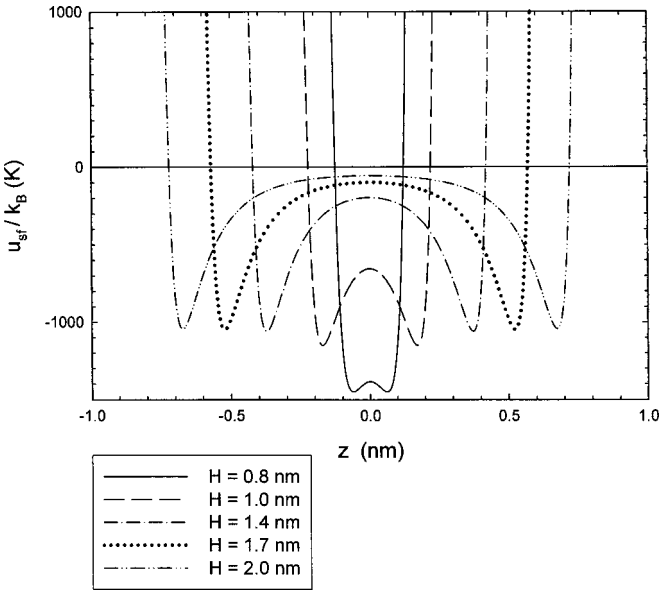

FIG. 1. Solid-fluid interaction potential, u_sf, for the NO monomer in the model carbon slit nanopore of various widths H; z is the distance of the NO molecule from the center of the nanopore which is located at $z=0$ and k_B is Boltzmann's constant.

C. Equilibrium constant

The RxMC method requires knowledge of the equilibrium constant K. For the NO dimerization reaction $2\mathrm{NO} \rightleftharpoons (\mathrm{NO})_2$, K is defined[23] as

$$K = \exp\left(-\frac{\mu^0_{(\mathrm{NO})_2} - 2\mu^0_\mathrm{NO}}{RT}\right), \tag{9}$$

where $\mu^0_i(T,P^0)$ is the molar standard chemical potential of species i at T and P^0, and R is the universal gas constant. The dependence of $\mu^0_i(T,P^0)$ on P^0 is usually suppressed, and $\mu^0_i(T)$ may be expressed as

$$\mu_i^0(T) = h_i^0(T) - Ts_i^0(T), \tag{10}$$

where the molar enthalpy, $h_i^0(T)$, and the molar entropy, $s_i^0(T)$, may be expressed as

$$h_i^0(T) = \Delta H_{fi}(T_r) + \int_{T_r}^{T} c_{pi}^0(T)dT, \tag{11}$$

$$s_i^0(T) = s_i^0(T_r) + \int_{T_r}^{T} \frac{c_{pi}^0(T)}{T}dT. \tag{12}$$

In Eqs. (11) and (12), $\Delta H_{fi}(T_r)$ is the enthalpy of formation of species i at the reference temperature T_r (taken to be 298.15 K) and c_{pi}^0 is its ideal-gas heat capacity.

In general, K refers to the isolated-molecule (ideal-gas) properties. The most accurate values for these properties are available in thermochemical tables such as the TRC or JANAF tables,[34,35] which are constructed using the most accurate available partition function (PF) data. Hence in this work, values of K at different T's were evaluated by means of the TRC thermochemical table[34] and Eqs. (9)–(12). In contrast, Turner *et al.*[6] and Johnson *et al.*[14] in their RxMC study of the NO dimerization system calculated K using the internal degrees of freedom of the NO and $(NO)_2$ molecules (translational, rotational, vibrational, and electronic) based on classical statistical mechanics.[36] In principal, both approaches should yield the same K values since μ_i^0 is related to the internal PF_i (Ref. 37) via

$$\mu_i^0 = -RT \ln\left(\frac{q_i^r q_i^v q_i^e}{\Lambda_i^3}\frac{k_B T}{P^0}\right). \tag{13}$$

In Eq. (13), Λ_i is the de Broglie thermal wavelength, and q_i^r, q_i^v, and q_i^e are, respectively, rotational, vibrational, and electronic contributions to the internal PF_i. However, due to a large variation in the literature values of the $(NO)_2$ dissociation energy D_0, which is needed for the evaluation of $q_{(NO)_2}$, Turner *et al.*[6] and Johnson *et al.*[14] adjusted the value of D_0 from a series of short simulation runs performed at 110 and 116 K, respectively. D_0 was adjusted until a reasonable agreement with the experimental data[38] of dimer concentrations in the bulk saturated liquid was found. Turner *et al.* obtained $D_0 = 10.9$ kJ/mol at $T = 110$ K and Johnson *et al.* obtained $D_0 = 13.6$ kJ/mol at $T = 116$ K; both values are within the wide range of D_0 values, 7.64–13.8 kJ/mol, reported in the literature.[39–42]

IV. RESULTS AND DISCUSSION

We performed the simulation study on the $2NO \rightleftharpoons (NO)_2$ system at low P's and T's from 110 to 170 K, and for nanopore widths $H = (0.8, 1.0, 1.4, 1.7, 2.0)$ nm. The experimental normal boiling point of the bulk system is 121.4 K and at this condition the system is almost completely monomeric in the vapor phase in contrast to many associating fluids such as acetic acid.[38] At the studied P's and T's, experiments and RxMC simulations show that the saturated-vapor phase contains about 0.01–0.02 mole fraction of dimers. In contrast to the saturated-vapor phase, the dimerization is pronounced in the liquid phase, as seen from Fig. 2. Figure 2 shows the mole fraction of liquid $(NO)_2$ along the experimental saturation line (P varies from 0.2 to 43.3 bars), as obtained from the experiments of Smith and Johnston,[38] from the RxMC simulations of Turner *et al.*[6] and Johnson *et al.*,[14] and from our RxMC simulations. Figure 2 shows nearly complete dimerization at low T's. Further, the degree of dimerization decreases with increasing T and at $T > 170$ K, the system becomes monomeric. We also see from Fig. 2 that despite the use of the same molecular model, our RxMC simulations predict a smaller degree of dimerization in comparison with the RxMC simulation results of Turner *et al.*[6] and Johnson *et al.*[14] This is a consequence of the differences in determining the equilibrium constant K, as discussed in Sec. III C. Since Turner *et al.*[6] and Johnson *et al.*[14] adjusted K to the experimental saturated-liquid composition at 110 and 116 K, respectively, their RxMC simulation results agree quite well with the experimental data measured by Smith and Johnston[38] at the temperature interval from 110 to 120 K. As previously noted by Johnson *et al.*[14] and which is also evident from a comparison of the RxMC simulation results of Turner *et al.*[6] and Johnson *et al.*[14] in Fig. 2, the simulation results are extremely sensitive to changes in K. We are not aware of any experimental data on the saturated-liquid $2NO \rightleftharpoons (NO)_2$ system at $T > 120$ K to shed more light on differences between these particular RxMC simulation results. However, we argue that the equilibrium constant should be determined *unambiguously*, as done in this work, by means of the most accurate data available in the standard thermochemical tables.

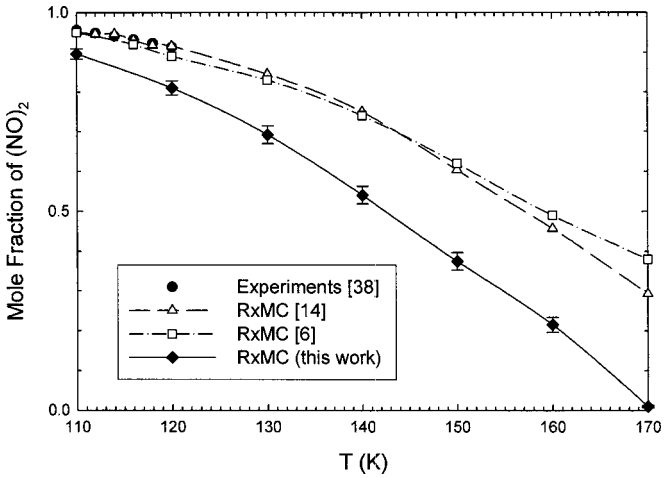

FIG. 2. Mole fraction of $(NO)_2$ dimers as a function of temperature T along the saturation line for the bulk liquid-phase $2NO \rightleftharpoons (NO)_2$ system from the RxMC simulations and from the experiments. The lines are drawn as a guide to the eye.

A. Effects of nanopore size

We investigated the influence of the nanopore width on reaction conversion by performing two-phase reaction simulations, which includes a bulk phase at pressure $P_{bulk} = 0.16$ bar in equilibrium with an adsorbed phase in a model carbon slit nanopore. Temperatures were varied from 120 to160 K. Due to the low value of P_{bulk}, the RxMC simu-

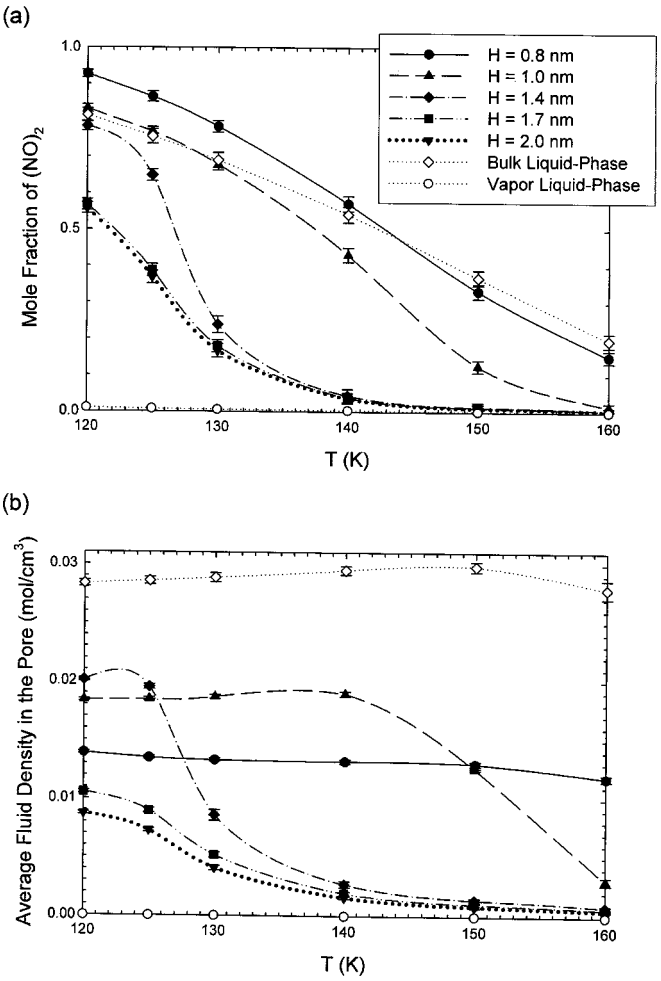

FIG. 3. (a) Mole fraction of $(NO)_2$ dimers and (b) average fluid density as a function of temperature T in the model carbon slit nanopore of various widths H at a bulk pressure of 0.16 bar. For comparison, the simulation results for the bulk vapor and liquid phases are also included. The lines are drawn as a guide to the eye.

lations showed that the bulk phase behaves as an ideal-gas system and is predominantly monomeric with about a 0.01–0.02 mole fraction of dimers.

Figure 3 reports the yield of dimers and the average fluid density in the pore for the confined NO dimerization reaction as a function of the nanopore width and temperature. For comparison, the simulation results for the bulk vapor and liquid phases at $P=0.16$ bar are included. Figure 3(a) shows a large enhancement of the dimer formation in the nanopores in comparison with the corresponding bulk vapor phase. The enhancement becomes greater as the nanopore width is reduced. For the nanopores with $H \geqslant 1.7$ nm, the influence of further increasing H becomes small. The previous studies of Turner *et al.*[6] and Tripathi and Chapman[18] resulted in similar findings.

The enhanced conversion is a result of two phenomena occurring simultaneously in the nanopore phase: (i) the increase in the average fluid density in the pore and (ii) the preferential adsorption of the $(NO)_2$ dimer on the nanopore surface. The enhanced conversion caused by the higher fluid density in the pore drives the reaction equilibrium towards the formation of more dimers, as seen in Fig. 3. For example, the density of the bulk vapor phase at $T=120$ K is about 0.16×10^{-4} mol/cm^3 while the corresponding average fluid density in the nanopores with $H=0.8$ and 2.0 nm is approximately 0.14×10^{-1} and 0.87×10^{-2} mol/cm^3, respectively. On the other hand, the average fluid density in the nanopores is substantially lower than the density of the bulk liquid phase while the reaction conversion in the nanopores with $H=0.8$ and 1.0 nm is comparable with that for the bulk liquid phase. This behavior is driven by the preferential adsorption of the dimer in the pore phase. The enhancement is further elucidated in plots of the solid-fluid interaction potentials u_{sf} in Fig. 1, in profiles of the NO and $(NO)_2$ densities given in Fig. 4, and in simulation snapshots shown in Fig. 5. As seen in Fig. 1, the overlap of the two strongly adsorbing wall potentials considerably lowers the energy in the nanopore. This effect is more pronounced in smaller nanopores, where values of u_{sf} near the nanopore center drop well below those for the larger nanopores. Hence for smaller nanopores, the fluid molecules near the nanopore center experience a strong interaction with both walls. Consequently, the fluid density in the nanopore center is high in these small nanopores [see, e.g., the fluid density profiles and simulation snapshot for $H=0.8$ nm in Figs. 4(a) and 5(a), respectively], contributing to a significantly higher dimer yield. The profiles of fluid densities in the smaller nanopores are more dependent on the variation in H due to the overlap of solid-fluid interaction potentials near the nanopore center, as seen for $H=0.8$, 1.0, and 1.4 nm in Figs. 4(a)–4(c) and 5(a)–5(c). Conversely for larger nanopores, the fluid molecules near the nanopore center experience a weak interaction with the walls and, thus, the fluid density near the nanopore center is small, as seen in Figs. 4(d) and 5(d) for the nanopore with $H=2.0$ nm. It should be also mentioned that the profiles of fluid densities for the nanopore with $H=1.7$ nm (not shown here) are very similar to those for the nanopore with $H=2.0$ nm. Hence for these larger nanopores, the effect of the confinement on the dimer yield is less strong and the dimer yield is not significantly affected by the variation in the nanopore width.

The other phenomena occurring in the nanopore phase that causes an enhanced conversion is the preferential adsorption of the $(NO)_2$ dimer on the nanopore surface. In other words, since the $(NO)_2$ dimer more strongly adsorbs inside the nanopore, the effect seen on the reaction equilibrium appears as a shift to a higher dimer formation inside the nanopore. Recall that the interaction energy between the $(NO)_2$ dimer and the nanopore surface is approximately twice as large as the NO monomer. However, since the size of the $(NO)_2$ dimer is approximately twice as large as the NO monomer, the relative sizes of the molecules can play a countereffect. The extent to which these effects balance can be seen from a closer examination of Figs. 4 and 5. In Figs. 4(a) and 5(a) for $H=0.8$ nm, it is clear that the $(NO)_2$ dimer strongly adsorbs in the center of the nanopore as a result of the influence of both nanopore surfaces. At this nanopore size there is little remaining available space in the nanopore for the NO monomer which can only adsorb on the nanopore surface. As the nanopore width is increased to $H=1.0$ nm, the profiles of fluid densities change dramatically, as seen in

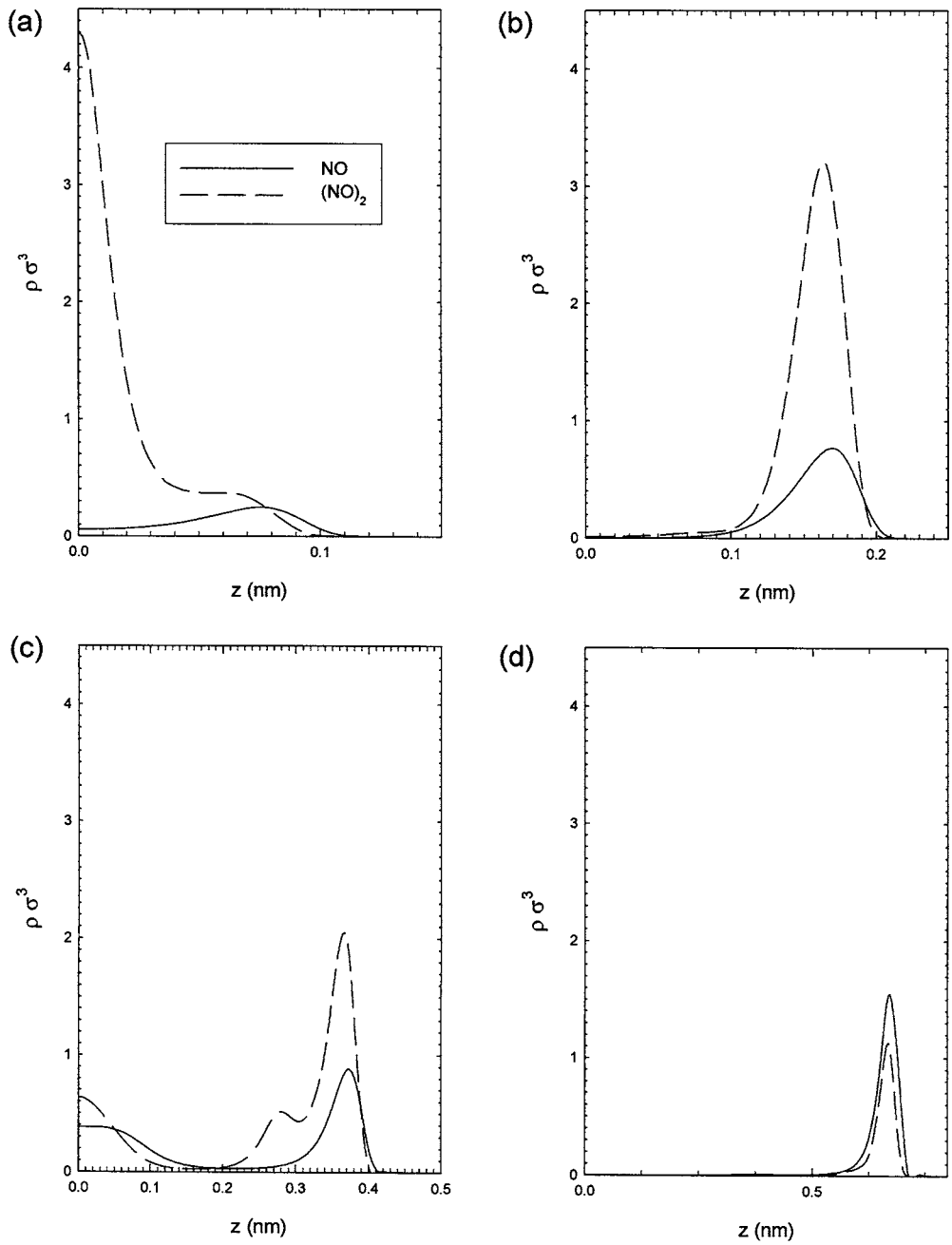

FIG. 4. Profiles of the NO- and $(NO)_2$-reduced densities, $\rho\sigma^3$, in the model carbon slit nanopore with widths of (a) $H=0.8$ nm, (b) $H=1.0$ nm, (c) $H=1.4$ nm, and (d) $H=2.0$ nm at a temperature of 125 K and at a bulk pressure of 0.16 bar; z is the distance from the center of the nanopore which is located at $z=0$. Due to nanopore symmetry, only half of the fluid density profiles are shown.

Figs. 4(b) and 5(b). The larger nanopore width allows for the formation of two layers. Now both species form layers on the nanopore surface with the more strongly attracted $(NO)_2$ dimer being the dominant species. From Figs. 4(c) and 5(c), we can see that as the nanopore width is further widened to $H=1.4$ nm, a third fluid layer emerges at the center of the nanopore. Here again the $(NO)_2$ dimer is the species which more strongly adsorbs shifting the reaction equilibria to the right. For the cases where $H=1.7$ and 2.0 nm, the profiles of fluid densities again change dramatically, as seen from Figs. 4(d) and 5(d) for $H=2.0$ nm. The nanopore is now so wide that fluid particles at the center of the nanopore do not experience the attraction of both surfaces, thus the third layer seen in Figs. 4(c) and 5(c) disappears. The profiles of fluid densities in Fig. 4(d) have well-defined peaks and are quite similar for both species. This is reflected in the equilibrium concentrations shown in Fig. 3(a).

The $(NO)_2$ yield in the nanopores is strongly influenced by the temperature (especially for $H=1.4$ nm), as further seen from Fig. 3. The reaction equilibrium conversion falls with increasing temperature, as observed in Fig. 3(a), since the NO dimerization reaction is exothermic and since an increase in T is accompanied by a decrease in the average fluid density in the pore, as shown in Fig. 3(b). This temperature effect is more pronounced than that seen in the bulk liquid phase.

Finally, Fig. 6 shows the one-dimensional self-diffusion coefficients, D^{NO} and $D^{(NO)_2}$, determined from *NVT* MD

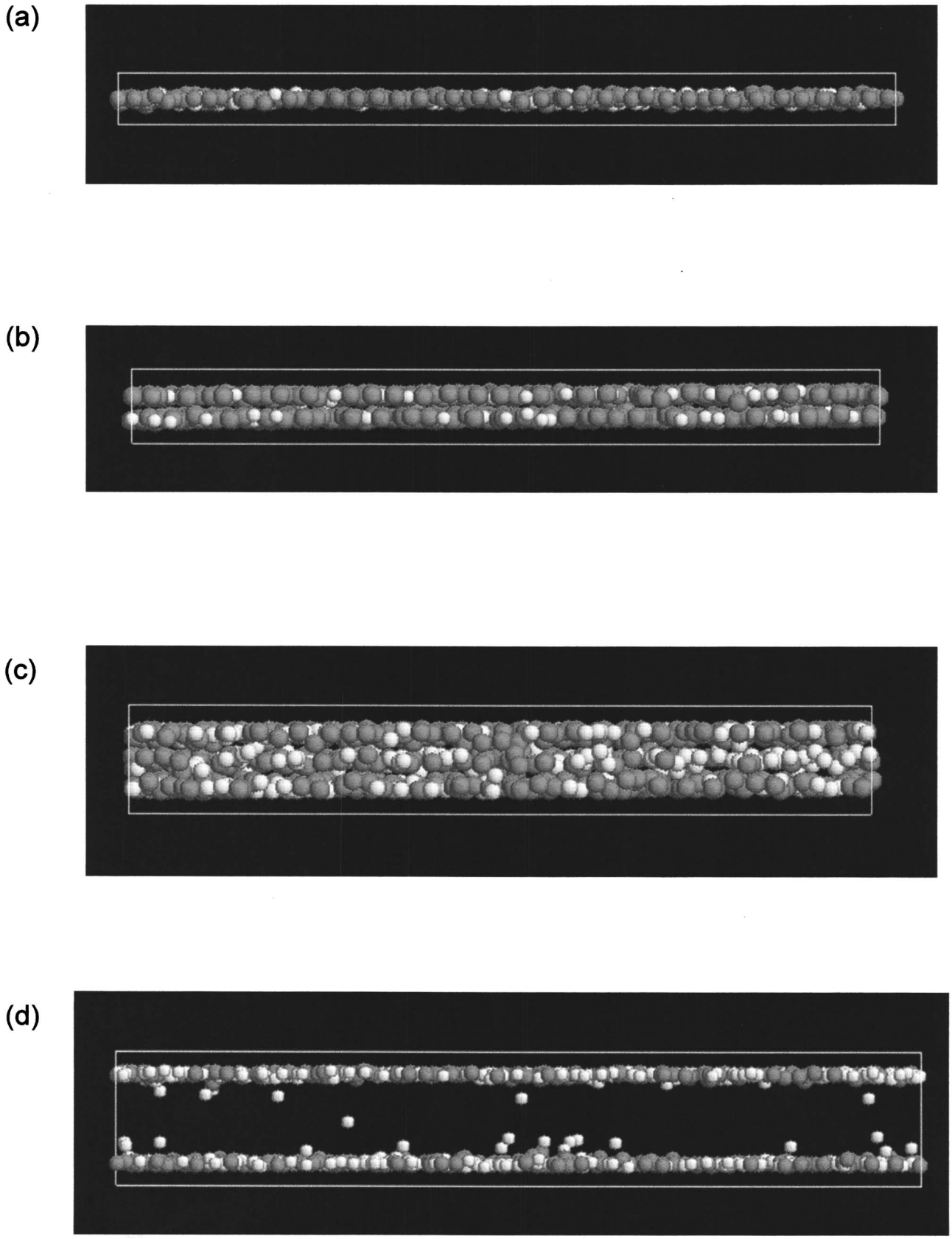

FIG. 5. Snapshots from RxMC simulations of the $NO/(NO)_2$ reactive mixture in the model carbon slit nanopore with widths of (a) $H=0.8$ nm, (b) $H=1.0$ nm, (c) $H=1.4$ nm, and (d) $H=2.0$ nm at a temperature of 125 K and at a bulk pressure of 0.16 bar. NO and $(NO)_2$ molecules are shown in white and red, respectively. The snapshots correspond to density profiles shown in Fig. 4.

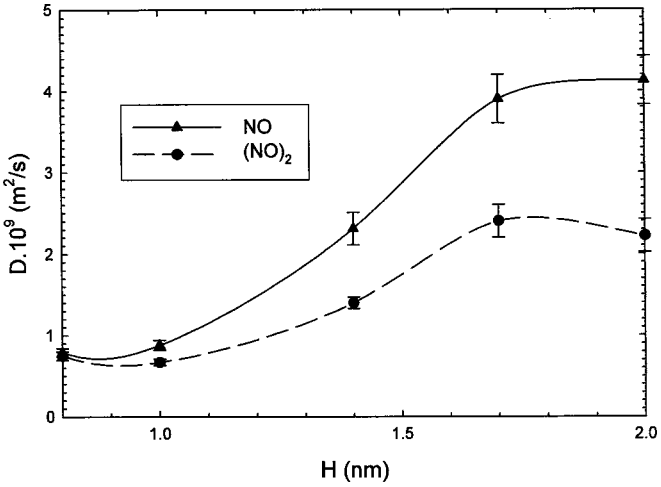

FIG. 6. One-dimensional self-diffusion coefficients for the NO monomers and $(NO)_2$ dimers, D^{NO} and $D^{(NO)_2}$, in the model carbon slit nanopore as a function of the nanopore width H at a temperature of 125 K and at a bulk pressure of 0.16 bar. The lines are drawn as a guide to the eye.

simulations of nonreactive mixtures in nanopores of various widths at $T=125$ K. As outlined in Sec. II B, the compositions are obtained from RxMC simulations and held constant during the *NVT* MD simulation. We see from Fig. 6 that at $H \leqslant 1.0$ nm, where $(NO)_2$ is the abundant component of the mixture and where the average fluid density in the pore increases with increasing H, values of D^{NO} and $D^{(NO)_2}$ are approximately the same and change only slightly with increasing H.

As the nanopore width is increased to 1.7 nm, both D^{NO} and $D^{(NO)_2}$ increase where the effect is greater for NO than for $(NO)_2$. Here, the mole fraction of $(NO)_2$ as well as the average fluid density in the pore decreases with increasing H. Finally, the self-diffusion coefficients for both species do not change significantly between $H=1.7$ and 2.0 nm when the system becomes mostly monomeric. The overall behavior exhibited in Fig. 6 is indicative of the shifting reaction equilibria with respect to the nanopore width.

B. Impact of bulk pressure and capillary condensation

We studied the influence of the bulk pressure and capillary condensation on the NO dimerization reaction equilibrium in model carbon slit nanopores with widths of 1.4, 1.7, and 2.0 nm at $T=125$ K. Bulk pressures, P_{bulk}, were varied from 0.16 bar up to the experimental vapor pressure of 1.50 bar.[38] Capillary condensation is a first-order transition that leads to the filling of nanopores with a phase characterized by a liquidlike density.[2] We found that the nanopore with $H=1.4$ nm is too small to exhibit capillary condensation while the nanopores with $H=1.7$ and 2.0 nm experience capillary condensation around $P_{bulk} \approx 0.4$ bar and $P_{bulk} \approx 0.7$ bar, respectively. These results are discussed in more detail below.

1. Model carbon slit nanopore with a width of 1.4 nm

Figure 7 shows the mole fraction of $(NO)_2$ dimers, the average fluid densities in the pore, and the one-dimensional self-diffusion coefficients as functions of the bulk pressure

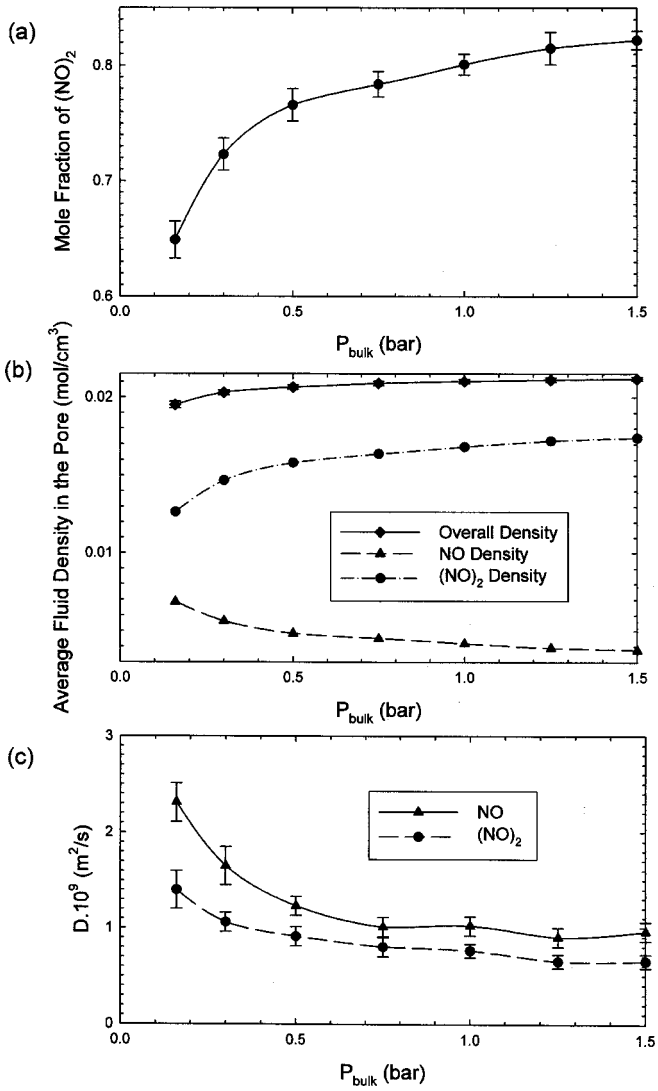

FIG. 7. (a) Mole fraction of $(NO)_2$ dimers, (b) average fluid densities in the pore, and (c) one-dimensional self-diffusion coefficients for the NO monomers and $(NO)_2$ dimers, D^{NO} and $D^{(NO)_2}$, as a function of bulk pressure P_{bulk} in the model carbon slit nanopore with a width of 1.4 nm at a temperature of 125 K. The symbols are simulation results of this work and the lines are drawn as a guide to the eye.

for the confined $2NO \rightleftharpoons (NO)_2$ system. We see from Fig. 7(a) that the reaction conversion increases with increasing P_{bulk} and that the increase is rather steep between 0.16 and 0.5 bar. The enhancement of the reaction conversion is driven by an increase in the overall average fluid density in the pore, as seen from Fig. 7(b). The enhancement in the $(NO)_2$ yield between $P_{bulk}=0.16$ bar and $P_{bulk}=1.50$ bar is about 20%, while the corresponding increase in the overall average fluid density in the pore is about 10%. The corresponding D^{NO} and $D^{(NO)_2}$ values plotted in Fig. 7(c) exhibit a decrease with increasing P_{bulk}, i.e., with an increasing overall average fluid density in the pore. The dependence of D^{NO} on P_{bulk} is the same as that for the average NO density in the pore, while the dependence of $D^{(NO)_2}$ on P_{bulk} is inverse to that of the average $(NO)_2$ density in the pore [cf. Fig. 7(c) with Fig. 7(b)]. The values of D^{NO} are higher than those of $D^{(NO)_2}$ despite the abundance of $(NO)_2$ in the reactive mixture at 125 K for these P_{bulk}'s. Figure 7(a) confirms the va-

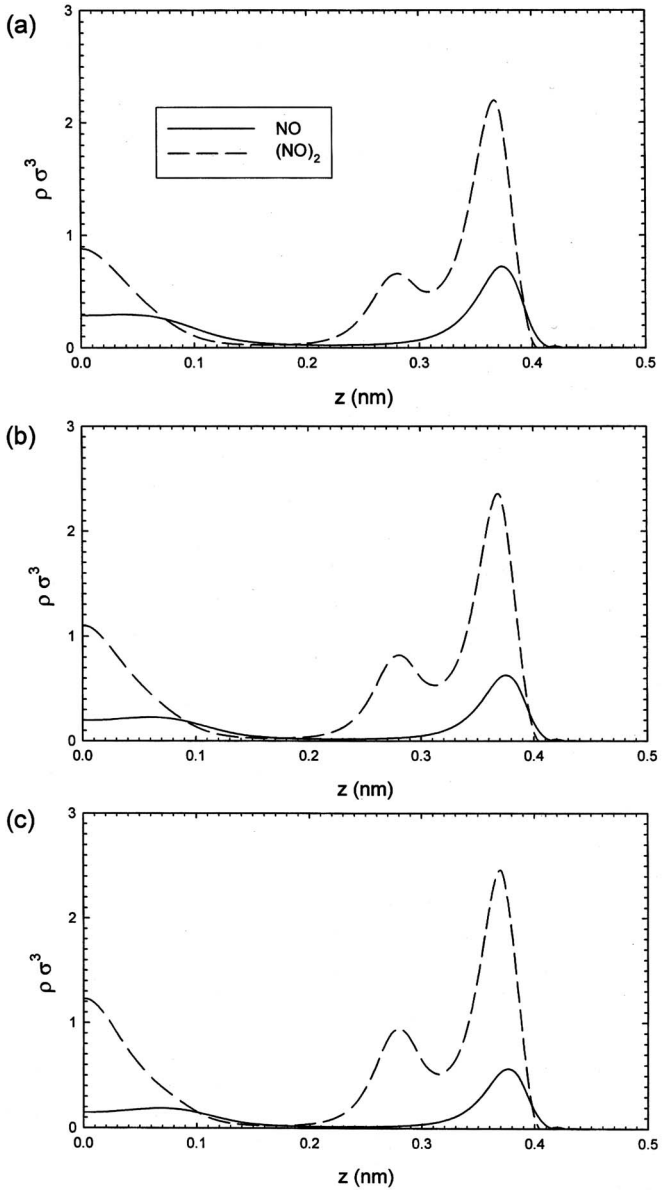

FIG. 8. Profiles of the NO- and $(NO)_2$-reduced densities, $\rho\sigma^3$, in the model carbon slit nanopore with a width of 1.4 nm at a temperature of 125 K and at bulk pressures of (a) 0.30, (b) 0.75, and (c) 1.50 bar; z is the distance from the center of the nanopore which is located at $z=0$. Due to nanopore symmetry, only half of the fluid density profiles are shown.

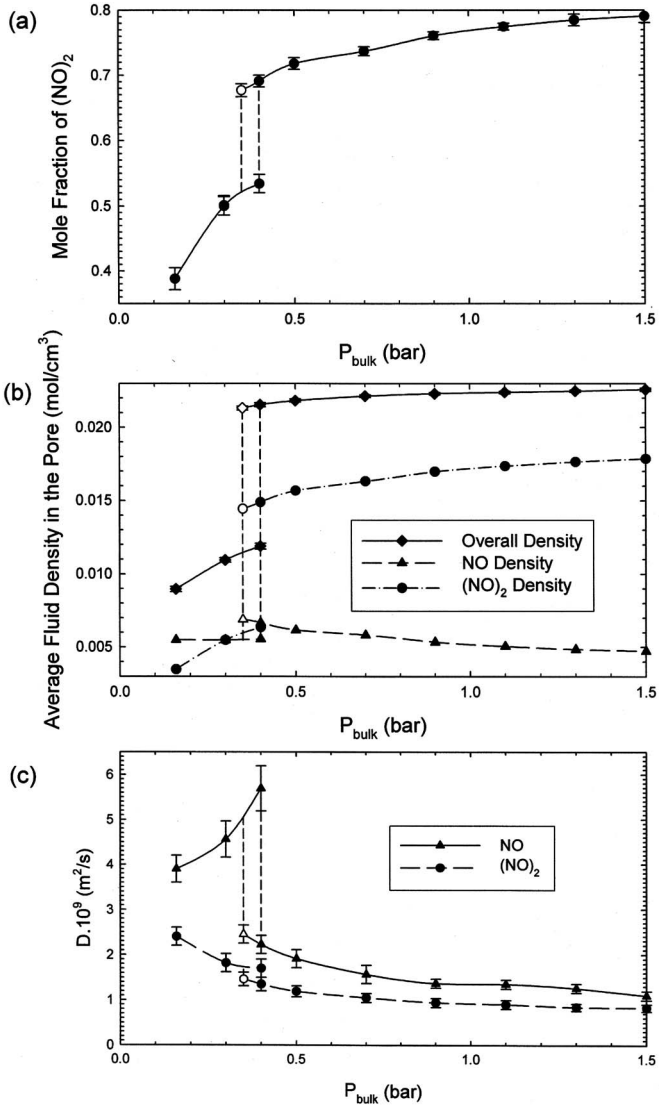

FIG. 9. (a) Mole fraction of $(NO)_2$ dimers, (b) average fluid densities in the pore, and (c) one-dimensional self-diffusion coefficients for the NO monomers and $(NO)_2$ dimers, D^{NO} and $D^{(NO)_2}$, as a function of bulk pressure P_{bulk} in the model carbon slit nanopore with a width of 1.7 nm at a temperature of 125 K. The symbols are simulation results of this work and the lines are drawn as a guide to the eye. The adsorption and desorption data points are shown as filled and open symbols, respectively.

lidity of applying Le Chatelier's principle to explain the behavior of the NO dimerization reaction equilibrium in slit nanopores: the equilibrium of a reactive system in which there is a decrease in the total number of moles shifts toward products when such a system experiences an increase in pressure.[23]

The impact of P_{bulk} on the structure of the confined reactive mixture of $NO/(NO)_2$ is shown in Fig. 8 where we plot profiles of NO and $(NO)_2$ densities in the pore for different values of P_{bulk}. We see from Fig. 8 that P_{bulk} does not affect the overall character of both profiles, i.e., a pronounced peak at ~0.37 nm corresponding to the location of the solid-fluid potential minimum and subsequent peaks which are a result of steric and packing effects. The values of P_{bulk} only influence the heights of these peaks, especially for $(NO)_2$, as seen, e.g., from a comparison of Figs. 8(a) and 8(c). It is evident that as the pressure increases the adsorbed layers become more defined, but only slightly. The stronger adsorbing $(NO)_2$ dimer layers the nanopore surfaces with a less defined third layer residing at the center of the nanopore, while the NO monomer adsorbs near the nanopore surface.

2. Model carbon slit nanopores with widths of 1.7 and 2.0 nm

Figures 9 and 10 report the yield of dimers, the average fluid densities, and the diffusion coefficients D^{NO} and $D^{(NO)_2}$ as a function of P_{bulk} for the $2NO \rightleftharpoons (NO)_2$ system in nanopores with $H=1.7$ and 2.0 nm. For both nanopore widths, we observe a steep vertical rise in the adsorption/desorption isotherms for the dimer mole fractions [Figs. 9(a) and 10(a)] and for the average fluid densities in the pore [Figs. 9(b) and

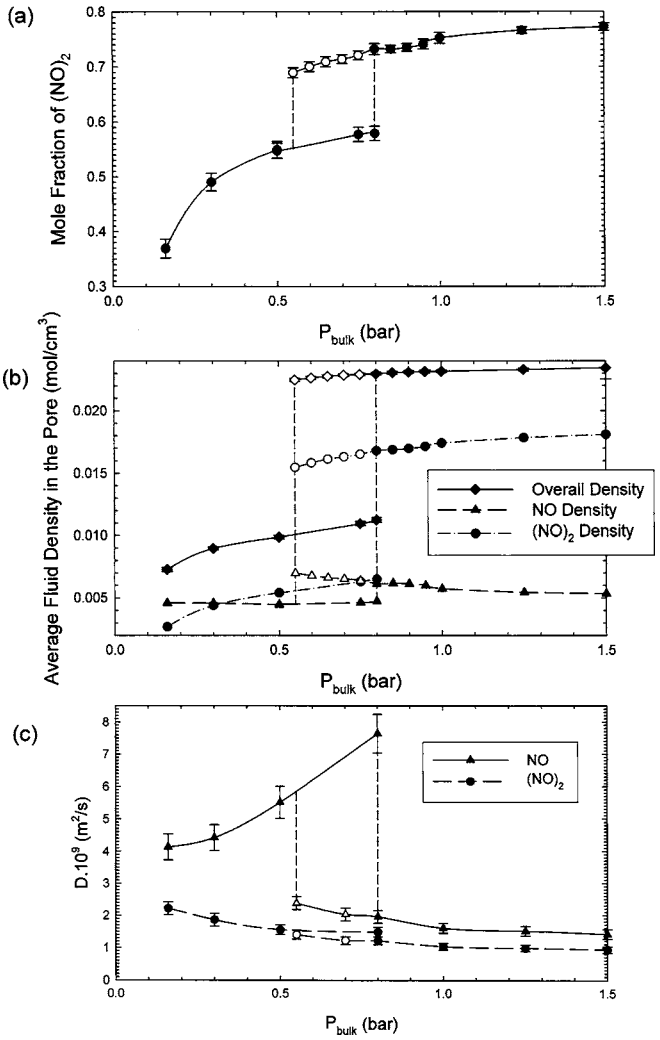

FIG. 10. (a) Mole fraction of $(NO)_2$ dimers, (b) average fluid densities in the pore, and (c) one-dimensional self-diffusion coefficients for the NO monomers and $(NO)_2$ dimers, D^{NO} and $D^{(NO)_2}$, as a function of bulk pressure P_{bulk} in the model carbon slit nanopore with a width of 2.0 nm at a temperature of 125 K. The symbols are simulation results of this work and the lines are drawn as a guide to the eye. The adsorption and desorption data points are shown as filled and open symbols, respectively.

10(b)] as a result of capillary condensation. Furthermore, hysteresis, widely regarded as the signature of capillary condensation,[2] is clearly evident in these isotherms. The bulk pressure at which capillary condensation occurs is lower in the smaller nanopore, while the hysteresis is broader in the larger nanopore. A dependence of D^{NO} and $D^{(NO)_2}$ on P_{bulk} [Figs. 9(c) and 10(c)] was also found. Discontinuities in these isotherms further suggest the occurrence of capillary condensation.

Closer inspection of Figs. 9 and 10 reveals some very interesting characteristics of the reactive system caused by capillary condensation. First, the reactants and products are in roughly equal proportion prior to capillary condensation for both nanopore widths, as seen from Figs. 9(a) and 10(a). However, after the onset of capillary condensation, the ratio of dimers to monomers changes to approximately 7:3 while reaching a ratio of 8:2 at the highest P_{bulk} considered. Another interesting characteristic is that the increase in the overall average fluid density in the pore as a result of capillary condensation is very nonuniformly distributed between the monomers and the dimers, as observed in Figs. 9(b) and 10(b). Beyond capillary condensation, the dependence of the average fluid densities in the pore on P_{bulk} is very similar to that found in the $H=1.4$ nm nanopore [cf. Figs. 9(b) and 10(b) with Fig. 7(b)]. Finally, quite unexpected behavior is the dependence of D^{NO} on P_{bulk} prior to capillary condensation, as seen in Figs. 9(c) and 10(c). Here, D^{NO} sharply increases with increasing P_{bulk}, while $D^{(NO)_2}$ decreases with increasing P_{bulk}. Beyond the onset of capillary condensation, the dependence of D^{NO} and $D^{(NO)_2}$ on P_{bulk} resembles the behavior found in the $H=1.4$ nm nanopore [cf. Figs. 9(c) and 10(c) with Fig. 7(c)].

The influence of capillary condensation on the structure of the confined reactive mixture of $NO/(NO)_2$ is elucidated in Figs. 11 and 12. Here, we display the profiles of the NO and $(NO)_2$ densities and simulation snapshots in the nanopore width $H=2.0$ nm at two bulk pressures prior to capillary condensation, $P_{bulk}=0.30$ and 0.75 bar [Figs. 11(a), 11(b), 12(a), and 12(b)], and at two bulk pressures after the onset of capillary condensation, $P_{bulk}=0.85$ and 1.50 bar [Figs. 11(c), 11(d), 12(c), and 12(d)]. It should be noted that the fluid density profiles in the nanopore width $H=1.7$ nm (not shown here) closely resemble fluid density profiles in the $H=2.0$ nm nanopore. Figures 11 and 12 clearly show the appearance and evolution of subsequent dense (condensation) layers of fluid molecules in the nanopore. The layer positioned around 0.7 nm from the nanopore center corresponds to the location of the solid-fluid potential minimum. The appearance of these subsequent dense layers is manifested by the presence of additional peaks in the fluid density profiles. For the precondensation case $P_{bulk}=0.30$ bar [Figs. 11(a) and 12(a)], the onset of another layer of NO molecules between 0.3 and 0.4 nm from the nanopore center is evident. Then just prior to capillary condensation, i.e., at $P_{bulk}=0.75$ bar, this additional NO layer becomes further pronounced while the onset of an additional layer of $(NO)_2$ molecules positioned also between 0.3 and 0.5 nm from the nanopore center can be seen in Figs. 11(b) and 12(b). Finally, after capillary condensation, these additional NO and $(NO)_2$ layers further evolve along with the appearance of layers of NO and $(NO)_2$ molecules in the nanopore center, as seen from Figs. 11(c), 11(d), 12(c), and 12(d).

V. CONCLUSIONS

The influence of confinement on chemical reaction equilibrium in nanoporous materials was studied in detail by means of reaction ensemble Monte Carlo and molecular-dynamics simulations for the nitric oxide dimerization reaction in model carbon slit nanopores. The effects of temperature, slit width, bulk pressure, and capillary condensation on the reaction conversion, fluid structure, and one-dimensional self-diffusion coefficients have been reported and discussed thoroughly.

A large increase in the dimerization in the nanopore phase was found with respect to the dimerization in the corresponding bulk phase. The dimerization increased by a factor of more than 80 for the smaller nanopores at the lower

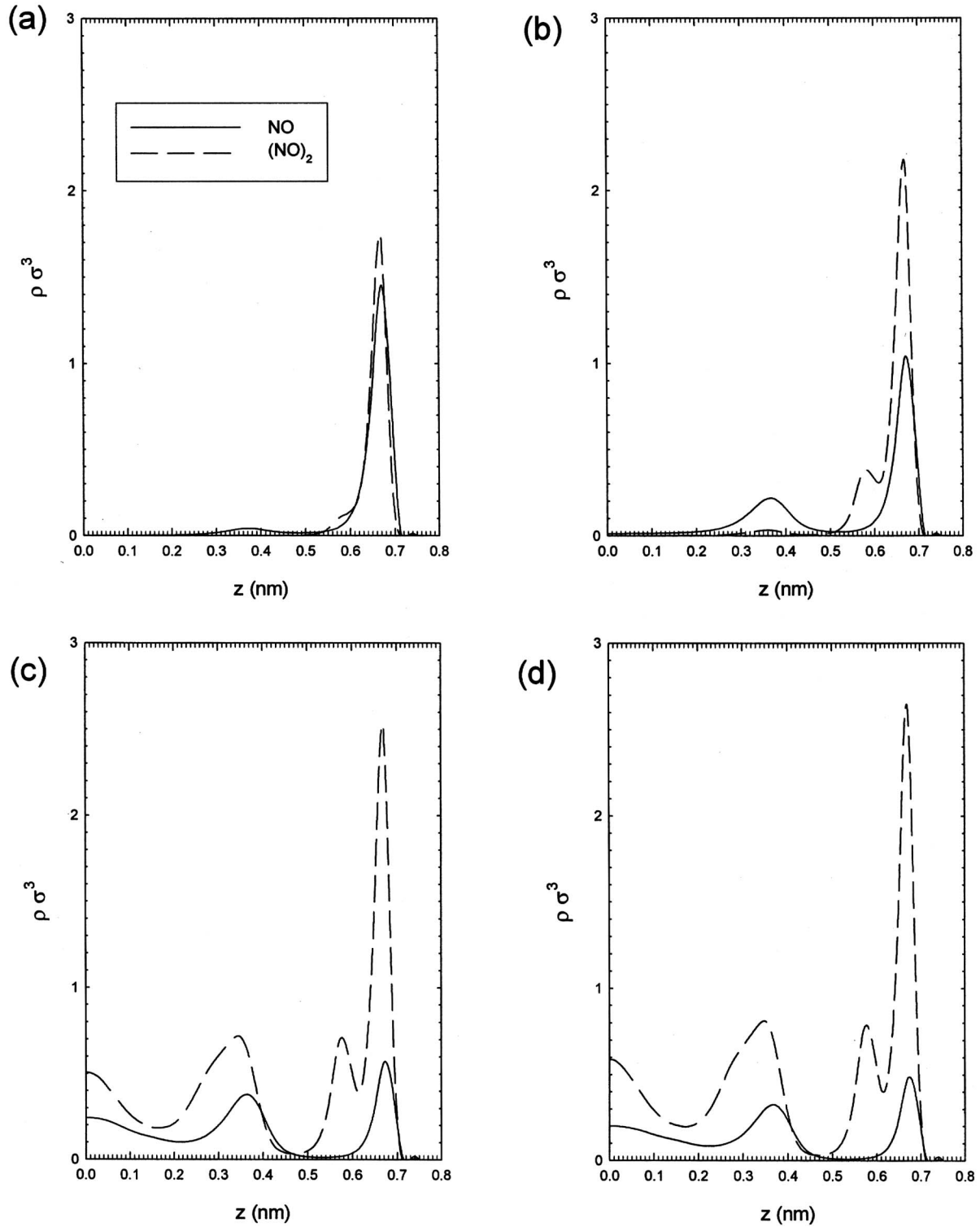

FIG. 11. Profiles of the NO- and $(NO)_2$-reduced densities, $\rho\sigma^3$, in the model carbon slit nanopore with a width of 2.0 nm at a temperature of 125 K and at bulk pressures of (a) 0.30 bar, (b) 0.75 bar (prior to capillary condensation), (c) 0.85 bar (after capillary condensation), and (d) 1.50 bars; z is the distance from the center of the nanopore which is located at $z=0$. Due to nanopore symmetry, only half of the fluid density profiles are shown.

temperatures and low pressure. The enhanced dimerization is due to the combined effects of the increased fluid density in the nanopore phase and the preferential adsorption of the $(NO)_2$ dimer in the nanopore. Analogous to the bulk phase behavior, the dimerization decreases with increasing temperature. The impact of the bulk phase pressure on the reaction conversion is moderate, unless capillary condensation occurs in the nanopores, in which case then is quite dramatic. The capillary condensation changes the ratio of dimers to monomers from roughly 1:1 prior to capillary condensation to a ratio of 7:3 after capillary condensation. This enhanced dimerization is caused by an increase in the overall fluid density in the nanopores. However, this increase is not distributed uniformly between monomers and dimers. There is a

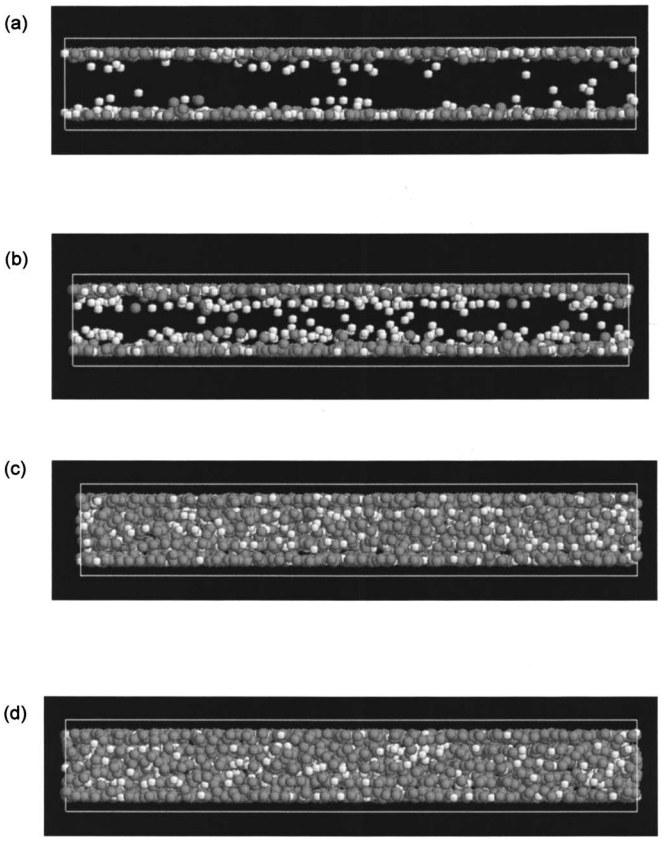

FIG. 12. Snapshots from RxMC simulations of the $NO/(NO)_2$ reactive mixture in the model carbon slit nanopore with a width of 2.0 nm at a temperature of 125 K and at bulk pressures of (a) 0.30 bar, (b) 0.75 bar (prior to capillary condensation), (c) 0.85 bar (after capillary condensation), and (d) 1.50 bar. NO and $(NO)_2$ molecules are shown in white and red, respectively. The snapshots correspond to density profiles shown in Fig. 11.

significantly larger increase in the average dimer density in the pore than in the average monomer density in the pore upon capillary condensation.

The magnetic susceptibility measurements of Kaneko *et al.*[9] and Nishi *et al.*[10] have found a much larger increase in dimerization due to confinement than the simulation studies.[6] Although the experiments and simulations in this work are performed at different thermodynamic conditions, some qualitative comparisons can be made. First, discrepancies may be due to experimental challenges in distinguishing between equilibrium states and long-lived metastable states in the nanopore. Second, other molecular species formed within the nanopore may be incorrectly interpreted as $(NO)_2$ dimers including complexes formed between the NO monomer and defects on the nanopore surface. While the intermolecular potential models used in the simulations are idealized, changes in the carbon-adsorbate interactions would need to be unrealistically large to match the experimental findings. For example, Turner estimated that the binding energy of the dimer would have to increase by a factor of 6 in order to approach the elevated conversions measured in the experiments.[43] An increase in the binding energy of this magnitude is unlikely. Moreover, the excellent quantitative agreement between simulation and DFT calculations[18] provides further justification for reconsidering the experimental results.

ACKNOWLEDGMENTS

This research was supported by the Grant Agency of the Czech Republic (Grant No. 203/05/0725), by the National Research Programme "Information Society" (Projects No. 1ET400720507 and 1ET100720409), and by the National Research Council of Canada (Grant No. OGP 1041).

[1] *Beyond the Molecular Frontier: Challenges for Chemistry and Chemical Engineering*, edited by R. Breslow and M. V. Tirrell (The National Academic Press, Washington, DC, 2003).
[2] L. D. Gelb, K. E. Gubbins, R. Radhakrishnan, and M. Sliwinska-Bartkowiak, Rep. Prog. Phys. **62**, 1573 (1999).
[3] T. J. Bandosz, M. J. Biggs, K. E. Gubbins, Y. Hattori, T. Iiyama, K. Kaneko, J. Pikunic, and K. T. Thomson, in *Chemistry and Physics of Carbon*, edited by L. R. Radovic (Marcel Dekker, New York, 2003), Vol. 28, pp. 41–228.
[4] M. Borówko, A. Patrykiejew, S. Sokołowski, R. Zagórski, and O. Pizio, Czech. J. Phys. **48**, 371 (1998).
[5] M. Borówko and R. Zagórski, J. Chem. Phys. **114**, 5397 (2001).
[6] C. H. Turner, J. K. Johnson, and K. E. Gubbins, J. Chem. Phys. **114**, 1851 (2001).
[7] C. H. Turner, J. Pikunic, and K. E. Gubbins, Mol. Phys. **99**, 1991 (2001).
[8] C. H. Turner, J. K. Brennan, J. K. Johnson, and K. E. Gubbins, J. Chem. Phys. **116**, 2138 (2002).
[9] K. Kaneko, N. Fukuzaki, K. Kakei, T. Suzuki, and S. Ozeki, Langmuir **5**, 960 (1989).
[10] Y. Nishi, T. Suzuki, and K. Kaneko, J. Phys. Chem. **101**, 1938 (1997).
[11] X. Peng, W. Wang, and S. Huang, Fluid Phase Equilib. **231**, 138 (2005).
[12] N. Hansen, S. Jakobtorweihen, and F. J. Keil, J. Chem. Phys. **122**, 164705 (2005).
[13] W. R. Smith and B. Tříska, J. Chem. Phys. **100**, 3019 (1994).
[14] J. K. Johnson, A. Z. Panagiotopoulos, and K. E. Gubbins, Mol. Phys. **81**, 717 (1994).
[15] M. Lísal, I. Nezbeda, and W. R. Smith, J. Chem. Phys. **110**, 8597 (1999).
[16] M. Lísal, J. K. Brennan, W. R. Smith, and F. R. Siperstein, J. Chem. Phys. **121**, 4901 (2004).
[17] J. K. Brennan, M. Lísal, K. E. Gubbins, and B. M. Rice, Phys. Rev. E **70**, 061103 (2004).
[18] S. Tripathi and W. G. Chapman, J. Chem. Phys. **118**, 7993 (2003).
[19] C. J. Segura and W. G. Chapman, Mol. Phys. **86**, 415 (1995).
[20] C. J. Segura, W. G. Chapman, and K. S. Shukla, Mol. Phys. **90**, 759 (1997).
[21] B. M. Rice, W. Mattson, J. Grosh, and S. F. Trevino, Phys. Rev. E **53**, 6184 (1985).
[22] S. J. Stuart, A. B. Tutein, and J. A. Harrison, J. Chem. Phys. **112**, 6472 (2000).
[23] W. R. Smith and R. W. Missen, *Chemical Reaction Equilibrium Analysis: Theory and Algorithms* (Wiley-Intersicence, New York, 1982;; *ibid*., reprinted with corrections (Krieger, Malabar, FL, 1991).
[24] M. P. Allen and D. J. Tildesley, *Computer Simulation of Liquids* (Clarendon, Oxford, 1987).
[25] D. Frenkel and B. Smit, *Understanding Molecular Simulation: From Algorithms to Applications* (Academic, London, 2002).
[26] S. C. McGrother and K. E. Gubbins, Mol. Phys. **97**, 955 (1999).
[27] I. Nezbeda and J. Kolafa, Mol. Simul. **14**, 153 (1995).
[28] K. P. Travis and K. E. Gubbins, Langmuir **15**, 6050 (1999).
[29] D. Brown and J. H. R. Clarke, Mol. Phys. **51**, 1243 (1984).
[30] D. Fincham, Mol. Simul. **8**, 165 (1992).
[31] H. J. C. Berendsen, J. P. M. Postma, W. F. van Gunsteren, A. DiNola, and J. R. Haak, J. Chem. Phys. **81**, 3684 (1984).
[32] F. Kohler, M. Bohn, J. Fischer, and R. Zimmermann, Monatsch. Chem. **118**, 169 (1987).
[33] W. A. Steele, *The Interaction of Gases with Solid Surfaces* (Pergamon, Oxford, 1974).
[34] J. B. Pedley, *Thermodynamical Data and Structures of Organic Compounds*, TRC Data Series Vol. I (Thermodynamic Research Center, College Station, TX, 1994).
[35] M. Chase, Jr., J. Phys. Chem. Ref. Data Monograph No. 9 (American Chemical Society, Washington, DC/AIP, New York, 1998).
[36] D. A. McQuarrie, *Statistical Mechanics* (University Science Books, New York, 2000).
[37] J. S. Rowlinson, *The Prefect Gas*, International Encyclopedia of Physical

Chemistry and Chemical Physics Vol. 5 (MacMillan Co., New York, 1963).
[38] A. L. Smith and H. L. Johnston, J. Am. Chem. Soc. **74**, 4696 (1952).
[39] B. J. Howard and A. R. W. McKellar, Mol. Phys. **78**, 55 (1993).
[40] A. R. W. McKeller and J. K. G. Watson, Mol. Phys. **86**, 273 (1995).
[41] A. Dkhissi, P. Soulard, A. Perrin, and N. Lacome, J. Mol. Spectrosc. **183**, 12 (1997).
[42] R. Gonzalez-Luque, M. Merchan, and B. O. Roos, Theor. Chim. Acta **88**, 425 (1994).
[43] C. H. Turner, Ph.D. thesis, North Carolina State University, 2002.

NO. OF COPIES	ORGANIZATION
1 (PDF ONLY)	DEFENSE TECHNICAL INFORMATION CTR DTIC OCA 8725 JOHN J KINGMAN RD STE 0944 FORT BELVOIR VA 22060-6218
1	US ARMY RSRCH DEV & ENGRG CMD SYSTEMS OF SYSTEMS INTEGRATION AMSRD SS T 6000 6TH ST STE 100 FORT BELVOIR VA 22060-5608
1	DIRECTOR US ARMY RESEARCH LAB IMNE ALC IMS 2800 POWDER MILL RD ADELPHI MD 20783-1197
3	DIRECTOR US ARMY RESEARCH LAB AMSRD ARL CI OK TL 2800 POWDER MILL RD ADELPHI MD 20783-1197

ABERDEEN PROVING GROUND

1	DIR USARL AMSRD ARL CI OK TP (BLDG 4600)

NO. OF
COPIES ORGANIZATION

ABERDEEN PROVING GROUND

5 DIR USARL
AMSRD ARL WM BD
J BRENNAN